Two-Dimensional Modular Chaotification System for Improving Chaos Complexity

Zhongyun Hua, *Member, IEEE,* Yinxing Zhang, Yicong Zhou, *Senior Member, IEEE*

Abstract—Chaotic systems are widely studied in various research areas such as signal processing and secure communication. Existing chaotic systems may have drawbacks such as discontinuous chaotic ranges and incomplete output distributions. These drawbacks may lead to the defects of some chaos-based applications. To accommodate these challenges, this paper proposes a two-dimensional (2D) modular chaotification system (2D-MCS) to improve the chaos complexity of any 2D chaotic map. Because the modular operation is a bounded transform, the improved chaotic maps by 2D-MCS can generate chaotic behaviors in wide parameter ranges while existing chaotic maps cannot. Three improved chaotic maps are presented as typical examples to verify the effectiveness of 2D-MCS. The chaos properties of one example of 2D-MCS are mathematically analyzed using the definition of Lyapunov exponent. Performance evaluations demonstrate that these improved chaotic maps have continuous and large chaotic ranges, and their outputs are distributed more uniformly than the outputs of existing 2D chaotic maps. To show the application of 2D-MCS, we apply the improved chaotic maps of 2D-MCS to secure communication. The simulation results show that these improved chaotic maps exhibit better performance than several existing and newly developed chaotic maps in terms of resisting different channel noise.

Index Terms—Chaotic system, chaotic signal, chaotification, dynamical system, secure communication

I. INTRODUCTION

IN the past few decades, nonlinear systems have received intensive attentions of researchers [1]–[3] and been applied to many application fields [4], [5]. As a branch of nonlinear science, chaos theory focuses on the behaviors that have sensitive dependence on initial states, for example, the well-known butterfly effect [6]. A chaotic system is a mathematical model to describe the chaotic behaviors. For a given initial state, a chaotic system is deterministic [7]. However, its trajectories are unpredictable when the initial state is unknown [8]. With this characteristic, a chaotic system can obtain many natural properties, including initial state sensitivity, topological transitivity and unpredictability [9], [10]. Such useful properties

Zhongyun Hua and Yinxing Zhang are with School of Computer Science and Technology, Harbin Institute of Technology, Shenzhen, Shenzhen 518055, China (e-mail: huazhongyun@hit.edu.cn; huazyum@gmail.com).

Yicong Zhou is with Department of Computer and Information Science, University of Macau, Macau 999078, China (e-mail: yicongzhou@um.edu.mo).

make chaotic systems widely applied to many engineering applications [11], [12], such as signal detection [13], [14] and secure communication [15]–[17].

However, with the fast development of computer technology and artificial intelligence, studies have established that some valuable information about the chaotic systems or their chaotic signals can be deduced according to little information of the systems [18]–[20]. These studies mainly focus on identifying the mathematical definitions of chaotic systems [21], [22], or on estimating their initial states [23], [24] and chaotic signals under some conditions [25]. For example, a hybrid regularized echo state network was introduced to predict the multivariate chaotic signals using the past observation states [26]. Generally, chaotic systems easily have above situations if they have drawbacks in discontinuous chaotic ranges and incomplete output distributions [27]. If some valuable information about the equation or chaotic signal of a chaotic system can be estimated, the system may lose the essential properties of chaos and this may cause negative impacts on its applications [28], [29].

As reviewed in [30], many works have been devoted to addressing the weaknesses of existing chaotic systems [31], [32]. One widely used strategy is to improve the complexity of chaotic signals via disturbing their system parameters [33] or via directly interfering their chaotic signals [34], [35] using some noise or random numbers. For example, Chen *et al.* use noise to scramble the output states of modified Logistic map in [36]. This method can obtain chaotic signals with high randomness. However, this strategy of improving the complexity of chaotic signals has some weaknesses. First, some technologies of this strategy use random numbers to scramble chaotic signals. In many applications, chaotic systems are used to generate pseudorandom numbers [27]. Improving complexity of chaotic signals in these applications makes no sense if we have already obtained random numbers [36]. Second, when the output states of a chaotic system are disturbed using noise or random numbers, the integrity of its mathematical models may be broken. This may make the chaotic system lose some natural properties. Another effective strategy aims at improving the chaos complexity of existing chaotic systems [37] or at generating new chaotic systems with more complex chaotic behaviors [38]. For example, in [39], Zhou *et al.* introduced a chaotic framework to produce new chaotic maps using two existing chaotic maps as seed maps. Experimental results show that the new chaotic maps generated by this framework have much better performance than some existing maps. However, most efforts of this strategy focus only on one-dimensional chaotic systems. Few works have

been devoted to improving the chaos complexity of two-dimensional (2D) or high-dimensional (HD) chaotic systems.

This paper introduces a 2D modular chaotification system (2D-MCS) to improve the chaos complexity of any 2D chaotic map. Many existing 2D chaotic maps have quite narrow chaotic ranges because their phase planes will become uncompacted with the increase of their system parameters. However, 2D-MCS performs a modular operation to the outputs of system in each unit time and can always compact the phase plane. As a result, 2D-MCS can significantly improve the chaos complexity and enlarge the chaotic ranges of existing 2D chaotic maps. The main contributions of this work can be summarized as follows.

1) We propose the 2D-MCS as a general chaotification framework to improve the chaos complexity of any 2D chaotic map. To demonstrate the effectiveness of 2D-MCS, as examples, we use this framework to enhance the chaos complexity of three existing 2D chaotic maps.

2) The chaos properties of one example of 2D-MCS are mathematically analyzed using the definition of Lyapunov exponent. Property studies show that these improved chaotic maps of 2D-MCS have fully distributed trajectories, and can display robust chaotic behaviors in a large parameter range whereas the existing maps cannot.

3) We quantitatively evaluate these improved chaotic maps using Lyapunov exponent, sample entropy, joint entropy and correlation dimension. The evaluation results demonstrate their complex chaotic behaviors.

4) To investigate the application of 2D-MCS, we apply these improved chaotic maps to secure communication. The simulation results demonstrate that these maps show better performance in resisting different channel noise than several existing and new chaotic maps.

The rest of this paper is organized as follows. Section II reviews three existing 2D chaotic maps. Section III introduces the proposed 2D-MCS and studies three cases of improved chaotic maps of 2D-MCS. Section IV evaluates the performance of these improved chaotic maps. Section V investigates the application of the improved chaotic maps in secure communication and Section VI concludes this paper.

II. EXISTING 2D CHAOTIC MAPS

This section briefly introduces three 2D chaotic maps and analyzes their properties. These maps are used as examples to show the effectiveness of 2D-MCS in Section III-B.

The Hénon map

$$\begin{cases} x_{n+1} = 1 - ax_n^2 + y_n \\ y_{n+1} = bx_n, \end{cases} \quad (1)$$

is named after Michel Hénon in 1976 [1], where a and b are its system parameters. The Hénon map is used as a prototype of 2D chaotic systems and it demonstrates classical chaotic behaviors when $a = 1.4$ and $b = 0.3$.

In [40], Zeraoulia and Sprott designed a simple 2D chaotic map, called the Zeraoulia-Sprott map,

$$\begin{cases} x_{n+1} = -ax_n/(1 + y_n^2) \\ y_{n+1} = x_n + by_n, \end{cases} \quad (2)$$
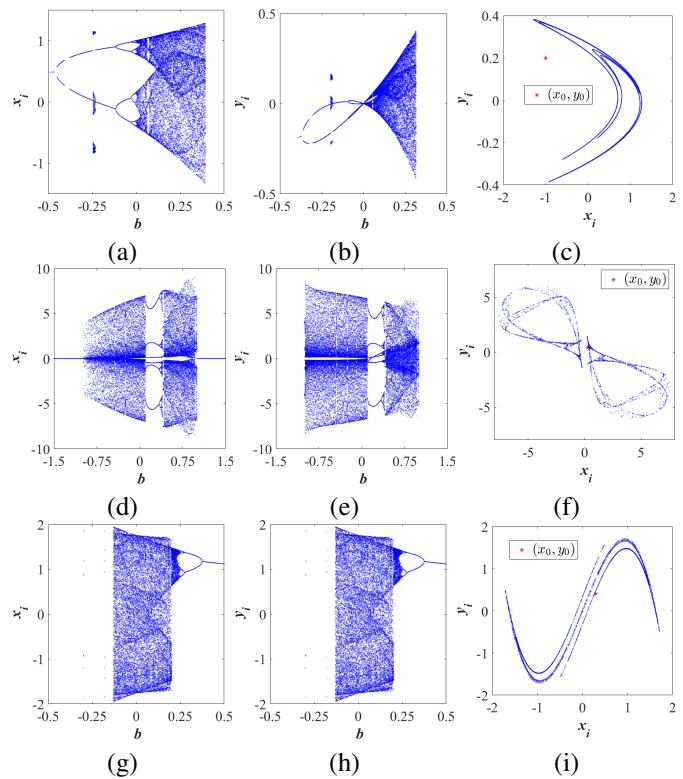

Fig. 1: Bifurcation diagrams and trajectories of three existing 2D chaotic maps. (a)-(c) Hénon map's bifurcation diagrams under $a = 1.4$ and $b \in (-0.5, 0.5)$, and its trajectory under $(a, b) = (1.4, 0.3)$; (d)-(f) Zeraoulia-Sprott map's bifurcation diagrams under $a = 3.8$ and $b \in (-1.5, 1.5)$, and its trajectory under $(a, b) = (3.8, 0.6)$; (g)-(i) Duffing map's bifurcation diagrams under $a = 2.75$ and $b \in (-0.5, 0.5)$, and its trajectory under $(a, b) = (2.75, 0.2)$.

where a and b are its system parameters. The Zeraoulia-Sprott map is characterized by one rational fraction and it shows classical chaotic behaviors when $a = 3.8$ and $b = 0.6$.

The Duffing map, also called Holmes map, is a widely used dynamical system of displaying chaotic behaviors [41]. Mathematically, the Duffing map is defined as

$$\begin{cases} x_{n+1} = y_n \\ y_{n+1} = -bx_n + ay_n - y_n^3, \end{cases} \quad (3)$$

where a and b are system parameters. When $a = 2.75$ and $b = 0.2$, the Duffing map shows classical chaotic behaviors.

The bifurcation diagram and trajectory of a dynamical system plot its visited or asymptotically visited states in the phase plane. They can reflect the behaviors of a dynamical system. Fig. 1 shows the bifurcation diagrams and trajectories of the Hénon, Zeraoulia-Sprott and Duffing maps. To better show the observation results, we plot their bifurcation diagrams with the change in the parameter b, and set the other parameter a as a fixed value that can make the corresponding chaotic map achieve classical chaotic behaviors. The parameters for generating the trajectories are also set as the values that can make the corresponding chaotic map achieve classical chaotic behaviors. For the Duffing map, as the state of variable x in next iteration equals to the current state of variable y, the bifurcation diagrams for variables x and y are the same, which can be seen from Figs. 1 (g) and (h).

From the mathematical equations, bifurcation diagrams and trajectories, one can observe that the Hénon, Zeraoulia-Sprott and Duffing maps have many notable properties. First, their chaotic ranges are discontinuous and even isolated. Small changes to their system parameters may shift the parameters into nonchaotic ranges. Second, their outputs distribute incompletely. Their trajectories only visit a small area of the phase plane and have prominent patterns. Moreover, their chaotic ranges are quite narrow. This means that they have chaotic behaviors only in limited parameter ranges. These properties may produce drawbacks in some chaos-based applications [29], [42]. Thus, overcoming these drawbacks of existing chaotic maps can promote chaos-based applications and is a meaningful research topic.

III. Two-Dimensional Modular Chaotification System

This section presents the two-dimensional modular chaotification system (2D-MCS), studies three examples of improved chaotic map by 2D-MCS and analyzes their chaos properties.

A. 2D-MCS

The 2D-MCS is proposed to accommodate the weaknesses of existing 2D chaotic maps in discontinuous, narrow chaotic ranges and incomplete output distributions. Using a modular operation as a bounded transformation and applying it to the outputs of an 2D chaotic map, the 2D-MCS can strongly improve the chaos complexity of such 2D chaotic map. The 2D-MCS can be represented as

$$\mathbf{M}(x, y) = \mathbf{F}(x, y) \mod N, \tag{4}$$

where x and y are two variables, the modulus coefficient N is a positive integer, and $\mathbf{F}(x, y)$ is a 2D chaotic map

$$\mathbf{F}(x, y) : \begin{cases} x_{n+1} = G(x_n, y_n) \\ y_{n+1} = H(x_n, y_n). \end{cases} \tag{5}$$

The iteration form of 2D-MCS in Eq. (4) can be written as

$$\mathbf{M}(x, y) : \begin{cases} x_{n+1} = G(x_n, y_n) \mod N \\ y_{n+1} = H(x_n, y_n) \mod N. \end{cases} \tag{6}$$

Many existing chaotic maps have chaotic behaviors only in small parameter ranges and cannot display chaos when their parameters increase to large values. This is because with the increase of their parameters, their phase planes will become uncompacted. This leads their output values to diverge to infinity with the evolution of the systems. However, 2D-MCS can always compact the phase plane because its modular operation is a bounded operation and can transform any input value into the range $[0, N)$. Such property makes the modular operation a natural candidate for improving the chaos complexity of chaotic maps. As a result, 2D-MCS can achieve the following properties. (1) It can greatly enlarge the chaotic ranges of existing chaotic maps. (2) It can generate robust chaotic behaviors in wide parameter ranges that existing chaotic maps show regular behaviors or even diverge. (3) As the 2D-MCS can increase the complexity of 2D chaotic maps,

the improved chaotic maps of 2D-MCS can generate outputs with full distributions in the phase plane.

B. Examples of 2D-MCS

To demonstrate the effectiveness of 2D-MCS, as examples, this section uses 2D-MCS to enhance the three 2D chaotic maps in Section II and studies the dynamics properties of the improved chaotic maps.

1) Improved Hénon Map: When applying 2D-MCS to improve the complexity of the Hénon map in Eq. (1), we can obtain the improved Hénon map as

$$\begin{cases} x_{n+1} = (1 - \hat{a}x_n^2 + y_n) \mod N \\ y_{n+1} = \hat{b}x_n \mod N, \end{cases} \tag{7}$$

where $\hat{a}$ and $\hat{b}$ are its two system parameters.

2) Improved Zeraoulia-Sprott Map: When using the Zeraoulia-Sprott map in Eq. (2) as $\mathbf{F}(x, y)$ in Eq. (4), we can obtain the improved Zeraoulia-Sprott map as

$$\begin{cases} x_{n+1} = -\hat{a}x_n/(1 + y_n^2) \mod N \\ y_{n+1} = (x_n + \hat{b}y_n) \mod N, \end{cases} \tag{8}$$

where $\hat{a}$, $\hat{b}$ are its two system parameters.

3) Improved Duffing Map: When applying 2D-MCS to the Duffing map in Eq. (3), one obtains the improved Duffing map

$$\begin{cases} x_{n+1} = y_n \mod N \\ y_{n+1} = (-\hat{b}x_n + \hat{a}y_n - y_n^3) \mod N, \end{cases} \tag{9}$$

where $\hat{a}$, $\hat{b}$ are its two system parameters.

The modulus coefficient N should be a positive integer and this work sets $N = 5$ in the examples of improved chaotic map. The two system parameters $\hat{a}$, $\hat{b}$ in these improved chaotic maps inherit from the parameters a, b in the original chaotic maps. The parameters a, b of these original chaotic maps have only narrow ranges. This is because the outputs of the chaotic maps will quickly diverge to infinity with the system evolution when their parameters are set as large values. However, as the modular operation in 2D-MCS is a bounded operation, the improved chaotic maps by 2D-MCS can always compact the phase plane. As a result, the two parameters $\hat{a}$, $\hat{b}$ in these improved chaotic maps can be any value. This work investigates the properties of these improved chaotic maps for the parameters $\hat{a}, \hat{b} \in [5, 100]$. One is flexible to set the modular coefficient N as other integers and set the system parameters $\hat{a}$, $\hat{b}$ as other data ranges.

C. Proof of Chaos

The Lyapunov exponent (LE) is a widely used indictor to prove the existence of chaos [43]. It measures the average divergence rate of two trajectories of a dynamical system starting from extremely close initial states. This work uses the definition of LE to prove the chaos of 2D-MCS. Because the definition of LE focuses on a dynamical system with specific expression, we take the improved Hénon map as an example of 2D-MCS. First, we give the definition of chaos in the sense of LE as Definition 1 [44].

Definition 1. *A dynamical system is chaotic in the sense of LE if it satisfies two conditions: 1) its phase plane is globally bounded; 2) it has at least one positive LE.*

If the dynamical system has more than one positive LE, it can acquire hyperchaotic behavior. The n LEs of an n-dimensional discrete-time dynamical system at initial state $\mathbf{x}_0$ can be calculated as [43]

$$LE_i = \lim_{k \to \infty} \frac{1}{k} \ln \gamma_i (\Phi_k), \quad i = 1, 2, \cdots, n \quad (10)$$

where $\gamma_i(\Phi_k)$ is the i-th eigenvalue of matrix Φ_k, $\Phi_k = \mathbf{J}(\mathbf{x}_0)\mathbf{J}(\mathbf{x}_1)\cdots\mathbf{J}(\mathbf{x}_{k-1})$, and $\mathbf{J}(\mathbf{x}_j)$ is the Jacobian matrix of the dynamical system at observation time j.

Suppose a 2D map

$$F(x, y) = \begin{pmatrix} f(x, y) \\ g(x, y) \end{pmatrix} \mod N$$

consists of two continuous maps $f(x, y)$ and $g(x, y)$. The $F(x, y)$ is discontinuous on the square $[0, N] \times [0, N]$, because the modular operation is a jump operation to obtain the remainder part. However, if a closed torus can be constructed by $F(x, y)$ with $[0, N] \times [0, N]$, the $F(x, y)$ is continuous on the torus (e.g. Chapter 2.7 on Page 93 of [45]). Fig. 2 shows the construction of torus by identifying the two pairs of opposite sides of the square. One can observe that a closed torus can be constructed when the left side align with the right side and the top side align with the bottom side. This indicates that the $F(x, y)$ is continuous on the torus if $F(0, y) = F(N, y)$ and $F(x, 0) = F(x, N)$.
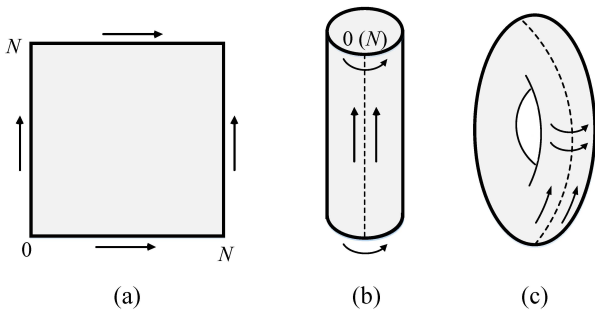

Fig. 2: Construction of a closed torus in two steps. (a) The square with size $[0, N] \times [0, N]$; (b) Glue together the vertical sides; (c) Glue together the horizontal sides.

A well-known example of such system is the Cat map. According to the discussions in Chapter 2.7 on Page 93 of [45], the Cat map $\begin{pmatrix} x_{n+1} \\ y_{n+1} \end{pmatrix} = \begin{pmatrix} 2x_n + y_n \\ x_n + y_n \end{pmatrix} \mod 1$ is continuous on a torus. This is because its values $(x_{n+1}, y_{n+1}) \in [0, 1] \times [0, 1]$ satisfy that $F(0, y_n) = F(1, y_n)$ and $F(x_n, 0) = F(x_n, 1)$, and a closed torus of unit size can be constructed. Then, the Cat map is differentiable on the torus and its Jacobian matrix $\mathbf{J}^{\text{Cat}} = \begin{pmatrix} 2 & 1 \\ 1 & 1 \end{pmatrix}$ (e.g. Page 197 of [45] and Page 316 of [46]). According to many literatures (e.g. Page 198 of [45]), the Cat map can satisfy the requirements of Definition 1 and it thus has chaotic behaviors on the torus. A modular system is chaotic if it has chaotic behavior on the torus (Page 198 of [47]).

For the improved Hénon map in Eq. (7) with values $(x_{n+1}, y_{n+1}) \in [0, N] \times [0, N]$, when its control parameters $\hat{a}$ and $\hat{b}$ are integers, it also satisfies that $F(0, y_n) = F(N, y_n)$ and $F(x_n, 0) = F(x_n, N)$. Then, a closed torus of size N can be constructed and the improved Hénon map is continuous on it. Since the torus constructed by the improved Hénon map is closed and smooth, the left partial derivative of the improved Hénon map always equals to its right partial derivative on $(0, N)$.

We introduce Proposition 1 that the improved Hénon map has chaotic behavior on the torus under specific parameter settings.

Proposition 1. *The improved Hénon map in Eq. (7) with integer control parameters $\hat{a}$ and $\hat{b}$ has chaotic behavior on the torus if its parameter $\hat{b}$ satisfy that $|\hat{b}| > 1$, and it has hyperchaotic behavior if its control parameters $\hat{a}$ and $\hat{b}$ satisfy that $|\hat{b}| > 1$ and $\hat{a} = 0$.*

Proof: Because the modular operation in the improved Hénon map is a bounded operation, the phase plane of the improved Hénon map is globally bounded. Then the condition 1) of Definition 1 is satisfied.

For the integer control parameters $\hat{a}$ and $\hat{b}$, the improved Hénon map is continuous on the torus and its Jacobian matrix can be derived as

$$\mathbf{J} = \begin{pmatrix} -2\hat{a}x & 1 \\ \hat{b} & 0 \end{pmatrix},$$

which is the same to that of the Hénon map in Eq. (1) with parameters a and b,

$$\mathbf{J}^{\text{Hénon}} = \begin{pmatrix} -2ax & 1 \\ b & 0 \end{pmatrix}.$$

Although the improved Hénon map and Hénon map have the same format of Jacobian matrix, their Jacobian matrix values are completely different due to the following two reasons. (1) Their output states are different; (2) Their parameters are different. The parameters $\hat{a}$ and $\hat{b}$ of the improved Hénon map can be any large values because the modular operation is a bounded operation, whereas the parameters a and b of the Hénon map have only narrow ranges because its output states will quickly diverge to infinity with large parameter values.

The multiplications of the Jacobian matrices of the improved Hénon map from observation time 0 to observation time $k-1$ can be calculated as

$$\Phi_k = \mathbf{J}(\mathbf{x}_0)\mathbf{J}(\mathbf{x}_1)\cdots\mathbf{J}(\mathbf{x}_{k-1})$$
$$= \begin{pmatrix} -2\hat{a}x_0 & 1 \\ \hat{b} & 0 \end{pmatrix} \begin{pmatrix} -2\hat{a}x_1 & 1 \\ \hat{b} & 0 \end{pmatrix} \cdots \begin{pmatrix} -2\hat{a}x_{k-1} & 1 \\ \hat{b} & 0 \end{pmatrix}$$
$$(11)$$

Let $\gamma_1(\Phi_k)$ and $\gamma_2(\Phi_k)$ be the two eigenvalues of Φ_k. According to the calculation of LE in Eq. (10), the two LEs of the improved Hénon map are

$$LE_1 = \lim_{k \to \infty} \frac{1}{k} \ln \gamma_1 (\Phi_k), \ LE_2 = \lim_{k \to \infty} \frac{1}{k} \ln \gamma_2 (\Phi_k). \quad (12)$$

Let the two eigenvalues of the matrix $\mathbf{J}(\mathbf{x}_j)$ be $\gamma_1(\mathbf{J}(\mathbf{x}_j))$ and $\gamma_2(\mathbf{J}(\mathbf{x}_j))$ $(j = 0, 1, \cdots, k-1)$. Since the determinant of the

Jacobian matrix $\mathbf{J}(\mathbf{x}_j)$ equals to $-\hat{b}$, one can obtain

$$\det(\mathbf{J}(\mathbf{x}_j)) = \gamma_1(\mathbf{J}(\mathbf{x}_j)) \cdot \gamma_2(\mathbf{J}(\mathbf{x}_j)) = -\hat{b}. \quad (13)$$

According to the properties of linear algebra, $\det(\mathbf{A_1 A_2} \cdots \mathbf{A_n}) = \det(\mathbf{A_1})\det(\mathbf{A_2}) \cdots \det(\mathbf{A_n})$ if $\mathbf{A_1}, \mathbf{A_2}, \cdots, \mathbf{A_n}$ are square matrices with the same size [48]. Then combining Eqs. (11) and (13), one gets

$$\begin{aligned}
\det(\Phi_k) &= \gamma_1(\Phi_k) \cdot \gamma_2(\Phi_k) \\
&= \det(\mathbf{J}(\mathbf{x}_0)) \cdot \det(\mathbf{J}(\mathbf{x}_1)) \cdots \det(\mathbf{J}(\mathbf{x}_{k-1})) \quad (14) \\
&= (-\hat{b})^k.
\end{aligned}$$

Combining with Eq. (12), one can obtain that

$$\begin{aligned}
LE_1 + LE_2 &= \lim_{k\to\infty} \frac{1}{k} \ln \gamma_1(\Phi_k) + \lim_{k\to\infty} \frac{1}{k} \ln \gamma_2(\Phi_k) \\
&= \lim_{k\to\infty} \frac{1}{k} \ln(\gamma_1(\Phi_k) \cdot \gamma_2(\Phi_k)) \quad (15) \\
&= \lim_{k\to\infty} \frac{1}{k} \ln(-\hat{b})^k \\
&= \ln(-\hat{b}).
\end{aligned}$$

It is obvious that when $|\hat{b}| > 1$, $LE_1 + LE_2 > 0$. Then at least one of LE_1 and LE_2 is positive. Notice that when the obtained LE value is a complex number, the LE is the real part, since the divergence of two close trajectories of a dynamical system is decided by the real part of the complex number [49], [50]. Then the condition 2) of Definition 1 is satisfied and the improved Hénon map has chaotic behavior.

Specially, when $|\hat{b}| > 1$ and $\hat{a} = 0$, the Jacobian matrix of the improved Hénon map becomes

$$\tilde{\mathbf{J}} = \begin{pmatrix} 0 & 1 \\ \hat{b} & 0 \end{pmatrix},$$

which is a constant matrix. Let γ_1 and γ_2 be the two eigenvalues of $\tilde{\mathbf{J}}$. One can obtain that $\gamma_1 = \sqrt{\hat{b}}$ and $\gamma_2 = -\sqrt{\hat{b}}$. Eq. (11) can be rewritten as

$$\Phi_k = \mathbf{J}(\mathbf{x}_0)\mathbf{J}(\mathbf{x}_1) \cdots \mathbf{J}(\mathbf{x}_{k-1}) = \tilde{\mathbf{J}}^k = \begin{pmatrix} 0 & 1 \\ \hat{b} & 0 \end{pmatrix}^k.$$

According to the properties of linear algebra, if λ_1 and λ_2 are the two eigenvalues of the 2×2 matrix $\mathbf{A}$, the two eigenvalues of $\mathbf{A}^n$ are λ_1^n and λ_2^n [48]. As $\gamma_1(\Phi_k)$ and $\gamma_2(\Phi_k)$ are the two eigenvalues of Φ_k, one can obtain that

$$\gamma_1(\Phi_k) = \gamma_1^k = (\sqrt{\hat{b}})^k, \quad \gamma_2(\Phi_k) = \gamma_2^k = (-\sqrt{\hat{b}})^k.$$

Combining with Eq. (12), one obtains that $LE_1 = \ln(\sqrt{\hat{b}})$ and $LE_2 = \ln(-\sqrt{\hat{b}})$. Since $|\hat{b}| > 1$, both of the LE_1 and LE_2 are larger than 0. Notice that when the obtained LE value is a complex number, the LE is the real part [49], [50]. This indicates that the improved Hénon map has two positive LEs and can achieve hyperchaotic behavior. The proof is completed. ∎

D. Stability

A fixed point is an element of a function domain that maps to itself by the function. For example, $\mathbf{v}$ is a fixed

point of $f(\cdot)$ if $f(f(\cdots f(\mathbf{v}) \cdots)) = \mathbf{v}$. The fixed points of the improved Hénon, improved Zeraoulia-Sprott and improved Duffing maps, denoted as $(\tilde{x}, \tilde{y})$, are the solutions of the following 2D equations:

$$\begin{cases} \tilde{x} = (1 - \hat{a}\tilde{x}^2 + \tilde{y}) \mod 5 \\ \tilde{y} = \hat{b}\tilde{y} \mod 5, \end{cases}$$

$$\begin{cases} \tilde{x} = -\hat{a}\tilde{x}/(1 + \tilde{y}^2) \mod 5 \\ \tilde{y} = (\tilde{x} + \hat{b}\tilde{y}) \mod 5, \end{cases}$$

and

$$\begin{cases} \tilde{x} = \tilde{y} \mod 5 \\ \tilde{y} = (-\hat{b}\tilde{x} + \hat{a}\tilde{y} - \tilde{y}^3) \mod 5, \end{cases}$$

respectively.

A fixed point of a dynamical system could be stable or unstable. A stable fixed point indicates that the states closing to the fixed point are attracted and the system is stationary in the long-term evolution. An unstable fixed point indicates that the fixed point rejects the closing states and that the system oscillates. The stability of a fixed point is determined by the system's gradient at the point. A 2D dynamical system has two gradients indicated by the two eigenvalues of its Jacobian matrix. Supposing that γ_1 and γ_2 are the two eigenvalues of the Jacobian matrix of a 2D dynamical system at a fixed point, the fixed point is locally stable if $|\gamma_1| < 1$ and $|\gamma_2| < 1$, and is unstable if $|\gamma_j| > 1$ for $j = 1$ or 2 [40]. Because the iterative values are with infinite precision, the Jacobian matrices of the improved Hénon, improved Zeraoulia-Sprott and improved Duffing maps are calculated as

$$\mathbf{J}(x, y) = \begin{pmatrix} -2\hat{a}x & 1 \\ \hat{b} & 0 \end{pmatrix},$$

$$\mathbf{J}(x, y) = \begin{pmatrix} -\hat{a}/(1 + y^2) & 2\hat{a}xy/(1 + y^2)^2 \\ 1 & \hat{b} \end{pmatrix},$$

and

$$\mathbf{J}(x, y) = \begin{pmatrix} 0 & 1 \\ -\hat{b} & \hat{a} - 3y^2 \end{pmatrix},$$

respectively.

Tables I, II and III list the fixed points and their absolute eigenvalues of the Jacobian matrices for the improved Hénon, improved Zeraoulia-Sprott and improved Duffing maps, respectively. One can see that these improved chaotic maps have different numbers of fixed points for different parameter settings. For all the fixed points, at least one absolute eigenvalue of the corresponding Jacobian matrix is larger than one. This implies that all the fixed points of the improved maps under these parameter settings are unstable.

Fig. 3 shows the bifurcation diagrams of the improved Hénon, improved Zeraoulia-Sprott and improved Duffing maps for $(\hat{a}, \hat{b}) \in [5, 100]$ and their trajectories under the parameter setting $(\hat{a}, \hat{b}) = (50, 50)$. As shown in Fig. 1, the Hénon, Zeraoulia-Sprott and Duffing maps have chaotic behaviors only within limited parameter ranges. With the change of parameters, these chaotic maps will step into chaotic states from regular states and can show how the systems route to chaos. Besides, the trajectories of these existing chaotic maps

TABLE I: Improved Hénon map's fixed points and the absolute eigenvalues of its Jacobian matrix at the fixed points.

$(\hat{a}, \hat{b})$	Fixed points $(\tilde{x}, \tilde{y})$	Absolute eigenvalues of $\mathbf{J}(\tilde{x}, \tilde{y})$
$(5, 5)$	$(3.1130, 0.5660)$	$\|\gamma_1\| = 31.2898, \|\gamma_2\| = 0.1598$
	$(2.2330, 1.1650)$	$\|\gamma_1\| = 22.5517, \|\gamma_2\| = 0.2217$
	$(2.4880, 2.4390)$	$\|\gamma_1\| = 25.0794, \|\gamma_2\| = 0.1994$
	$(4.8000, 4.0000)$	$\|\gamma_1\| = 48.1039, \|\gamma_2\| = 0.1039$
$(5, 6)$	$(1.7040, 0.2230)$	$\|\gamma_1\| = 17.3851, \|\gamma_2\| = 0.3451$
	$(1.1710, 2.0270)$	$\|\gamma_1\| = 12.2017, \|\gamma_2\| = 0.4917$
$(6, 5)$	$(4.2420, 1.2100)$	$\|\gamma_1\| = 51.0020, \|\gamma_2\| = 0.0980$
	$(4.9280, 4.6400)$	$\|\gamma_1\| = 59.2004, \|\gamma_2\| = 0.0844$
$\vdots$	$\vdots$	$\vdots$

TABLE II: Improved Zeraoulia-Sprott map's fixed points and the absolute eigenvalues of its Jacobian matrix at the fixed points.

$(\hat{a}, \hat{b})$	Fixed points $(\tilde{x}, \tilde{y})$	Absolute eigenvalues of $\mathbf{J}(\tilde{x}, \tilde{y})$
$(5, 5)$	$(3, 0.5)$	$\|\gamma_1\| = 4.9635, \|\gamma_2\| = 5.9635$
	$(2.2680, 0.6830)$	$\|\gamma_1\| = 4.1930, \|\gamma_2\| = 5.7835$
	$(3.9610, 1.5100)$	$\|\gamma_1\| = 2.2872, \|\gamma_2\| = 5.7629$
	$(2.3990, 1.9000)$	$\|\gamma_1\| = 1.4187, \|\gamma_2\| = 5.3341$
	$(3.2850, 2.9290)$	$\|\gamma_1\| = 0.7058, \|\gamma_2\| = 5.1838$
	$(3.8760, 4.0310)$	$\|\gamma_1\| = 0.3873, \|\gamma_2\| = 5.0975$
$(5, 6)$	$(1.1990, 0.7600)$	$\|\gamma_1\| = 3.5527, \|\gamma_2\| = 6.3833$
	$(4.5600, 1.0880)$	$\|\gamma_1\| = 3.3968, \|\gamma_2\| = 7.1072$
	$(2.0650, 1.5870)$	$\|\gamma_1\| = 1.7621, \|\gamma_2\| = 6.3410$
	$(3.9460, 4.2110)$	$\|\gamma_1\| = 0.3416, \|\gamma_2\| = 6.0747$
$(6, 5)$	$(2.7150, 0.5710)$	$\|\gamma_1\| = 5.5295, \|\gamma_2\| = 6.0048$
	$(1.2030, 0.9490)$	$\|\gamma_1\| = 3.5980, \|\gamma_2\| = 5.4411$
	$(4.7120, 1.3220)$	$\|\gamma_1\| = 3.3670, \|\gamma_2\| = 6.1834$
$\vdots$	$\vdots$	$\vdots$

TABLE III: Improved Duffing map's fixed points and the absolute eigenvalues of its Jacobian matrix at the fixed points.

$(\hat{a}, \hat{b})$	Fixed points $(\tilde{x}, \tilde{y})$	Absolute eigenvalues of $\mathbf{J}(\tilde{x}, \tilde{y})$
$(5, 5)$	$(1.5160, 1.5160)$	$\|\gamma_1\| = 2.2361, \|\gamma_2\| = 2.2361$
	$(2, 2)$	$\|\gamma_1\| = 0.8074, \|\gamma_2\| = 6.1926$
	$(3, 3)$	$\|\gamma_1\| = 0.2297, \|\gamma_2\| = 21.7703$
	$(4.3210, 4.3210)$	$\|\gamma_1\| = 0.0982, \|\gamma_2\| = 50.9149$
$(5, 6)$	$(1.3280, 1.3280)$	$\|\gamma_1\| = 2.4495, \|\gamma_2\| = 2.4495$
	$(1.8480, 1.8480)$	$\|\gamma_1\| = 1.6955, \|\gamma_2\| = 3.5387$
	$(2.8930, 2.8930)$	$\|\gamma_1\| = 0.3029, \|\gamma_2\| = 19.8054$
	$(3.8550, 3.8550)$	$\|\gamma_1\| = 0.1522, \|\gamma_2\| = 39.4309$
	$(4.4980, 4.4980)$	$\|\gamma_1\| = 0.1079, \|\gamma_2\| = 55.5881$
$(6, 5)$	$(0.1710, 0.1710)$	$\|\gamma_1\| = 1.0226, \|\gamma_2\| = 4.8897$
	$(1.7100, 1.7100)$	$\|\gamma_1\| = 2.261, \|\gamma_2\| = 2.2361$
	$(2.1550, 2.1550)$	$\|\gamma_1\| = 0.6918, \|\gamma_2\| = 7.2273$
	$(2.9240, 2.9240)$	$\|\gamma_1\| = 0.2578, \|\gamma_2\| = 19.3915$
	$(3.5560, 3.5560)$	$\|\gamma_1\| = 0.1572, \|\gamma_2\| = 31.7995$
	$(3.6840, 3.6840)$	$\|\gamma_1\| = 0.1446, \|\gamma_2\| = 34.5709$
	$(3.9140, 3.9140)$	$\|\gamma_1\| = 0.1255, \|\gamma_2\| = 39.8562$
	$(4.5620, 4.5620)$	$\|\gamma_1\| = 0.0887, \|\gamma_2\| = 56.3742$
	$(4.8620, 4.8620)$	$\|\gamma_1\| = 0.0771, \|\gamma_2\| = 64.8692$
$\vdots$	$\vdots$	$\vdots$

can visit only a small region in the phase plane and thus have strange behaviors. However, as can be seen from Fig. 3, variables x and y in the improved chaotic maps can randomly visit the entire regions of phase plane under all given parameter settings. Thus these improved chaotic maps do not have the parameter settings that make the chaotic maps step into chaotic states from regular ranges, and cannot exhibit how to route to chaos. In addition, the outputs of these improved chaotic maps can randomly distribute on the whole phase plane. This indicates that these improved chaotic maps can achieve robust chaotic behaviors. From this viewpoint, the improved chaotic maps by 2D-MCS have more complex chaotic behaviors and much larger chaotic ranges than the original chaotic maps. With uniformly distributed outputs, the improved chaotic maps are suitable for many applications such as the pseudo-random number generator.
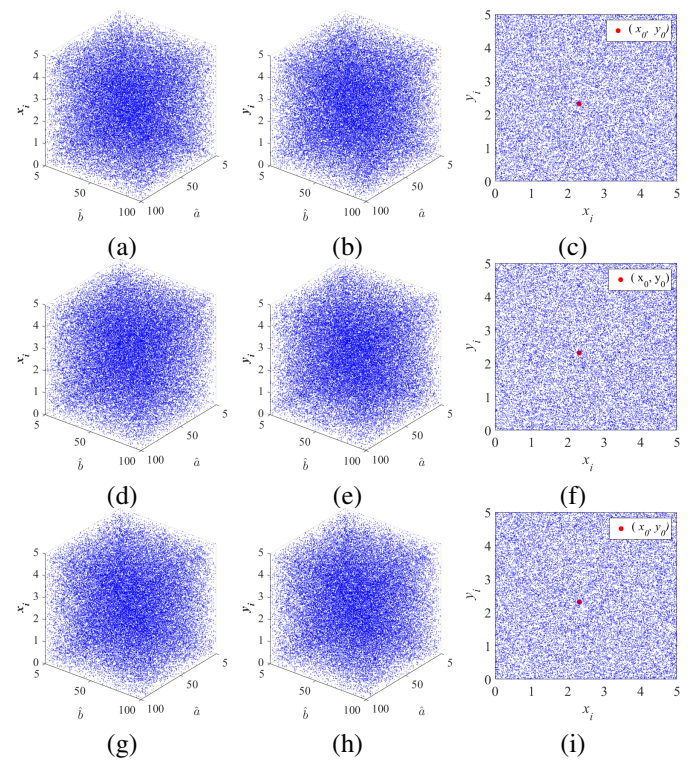

Fig. 3: Bifurcation diagrams and trajectories of (a)-(c) the improved Hénon map, (d)-(f) the improved Zeraoulia-Sprott map, and (g)-(i) the improved Duffing map.

IV. PERFORMANCE EVALUATIONS

This section quantitatively evaluates the chaotic behaviors of the three improved chaotic maps by 2D-MCS. The evaluations are performed from four aspects: LE, sample entropy (SE), joint entropy (JE) and correlation dimension (CD).

A. LE

As mentioned in Section III-C, the LE measures the average divergence rate of two trajectories of a dynamical system starting from extremely close initial states. A positive LE indicates that the two trajectories exponentially diverge in each unit time and thus the dynamical system is sensitive to initial
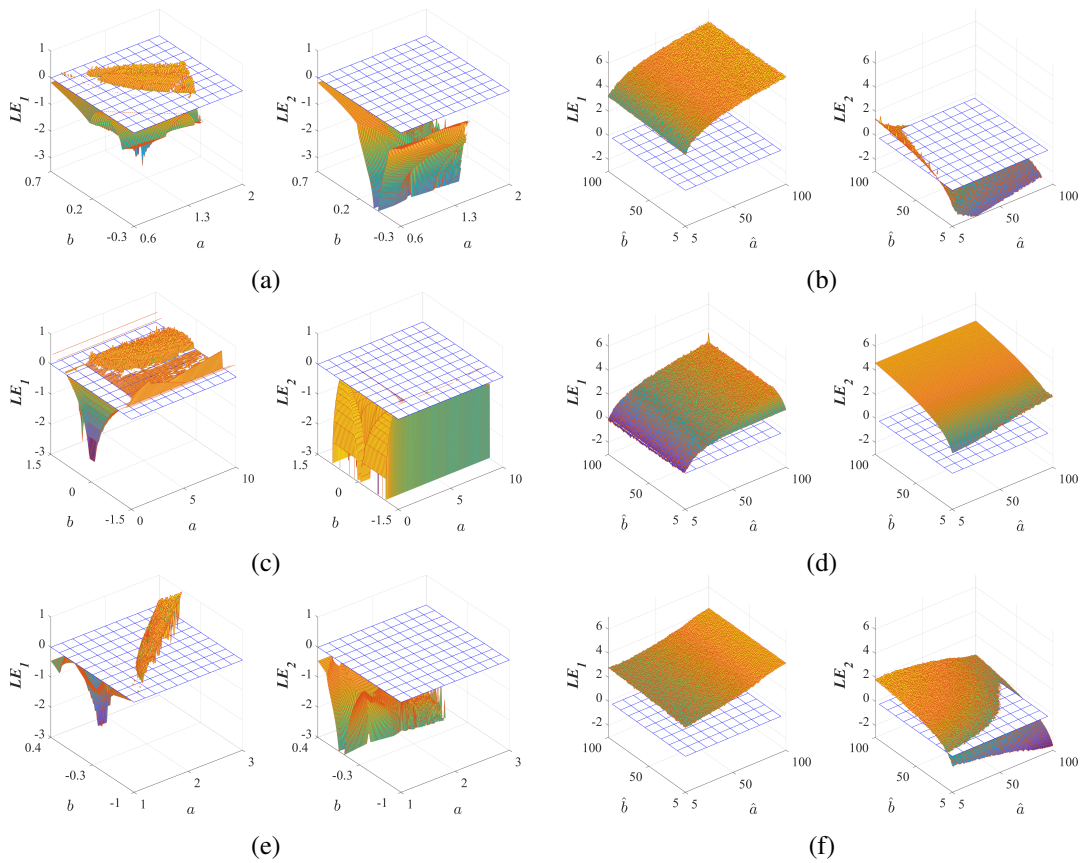
Fig. 4: Two LEs of different 2D chaotic maps. (a) Hénon map; (b) improved Hénon map; (c) Zeraoulia-Sprott map; (d) improved Zeraoulia-Sprott map; (e) Duffing map; (f) improved Duffing map.

states. Thus, a positive LE is an indicator of chaos if the phase plane of the dynamical system is compacted, and a larger LE indicates a higher sensitivity to initial states [44]. If a system has several positive LEs, its close trajectories diverge in several directions, making the system achieve hyperchaotic behaviors. The hyperchatic behavior is a more complex dynamic behavior than the chaotic behavior.

Our experiments use the LE calculation toolbox LET[1] to calculate the LEs of chaotic maps and Fig. 4 plots the calculated LEs of the improved and existing 2D chaotic maps. One can observe that the three improved chaotic maps not only have positive LEs in all the parameter settings, but also can obtain two positive LEs in large parameter regions. In particularly, the improved Zeraoulia-Sprott maps have two positive LEs almost in the whole parameter ranges. As comparison, the Hénon, Zeraoulia-Sprott and Duffing maps obtain positive LEs only in small parameter ranges, and their chaotic ranges are discontinuous or even isolated. Besides, the improved chaotic maps have much larger LEs than the existing maps. Fig. 4 plots the two LEs of the improved chaotic maps only within the parameter range $[5, 100]$. These improved chaotic maps always have positive LEs when their system parameters increase to any large value. This indicates that 2D-MCS can significantly enlarge the chaotic ranges and improve the chaos complexity of existing 2D chaotic maps.

[1] https://ww2.mathworks.cn/matlabcentral/fileexchange/233-let? requestedDomain=zh

B. SE

The SE can measure the degree of complexity of a time series [51]. A larger positive SE means the lower regularity of the time series. When the measured time series are generated by a chaotic system, the larger positive SE indicates the higher complexity of the system.

When calculating the SEs of different chaotic maps, our experiments set m as 2 and r as $0.2 \times std$, where std is the standard deviation of the time series, in accordance with [51]. Fig. 5 plots the SEs of the three improved 2D chaotic maps and three existing chaotic maps with different parameter settings. One can observe that the improved chaotic maps can always generate time series with positive SEs and their generated SEs are much larger than the SEs of time series generated by the existing chaotic maps. These results are consistent with the LE experiment results in Fig. 4 and prove that the three improved chaotic maps have high dynamic complexity.

C. JE

The JE characterizes the uncertainty and randomness of several signals. For a set of signals $\{S_1, S_2, \cdots, S_K\}$ with M states in each signal, the JE is defined as

$$H(S_1 S_2 \cdots S_K) = -\sum_{i_1=1}^{M} \sum_{i_2=1}^{M} \cdots \sum_{i_K=1}^{M} P(b_{i_1} b_{i_2} \cdots b_{i_K})$$
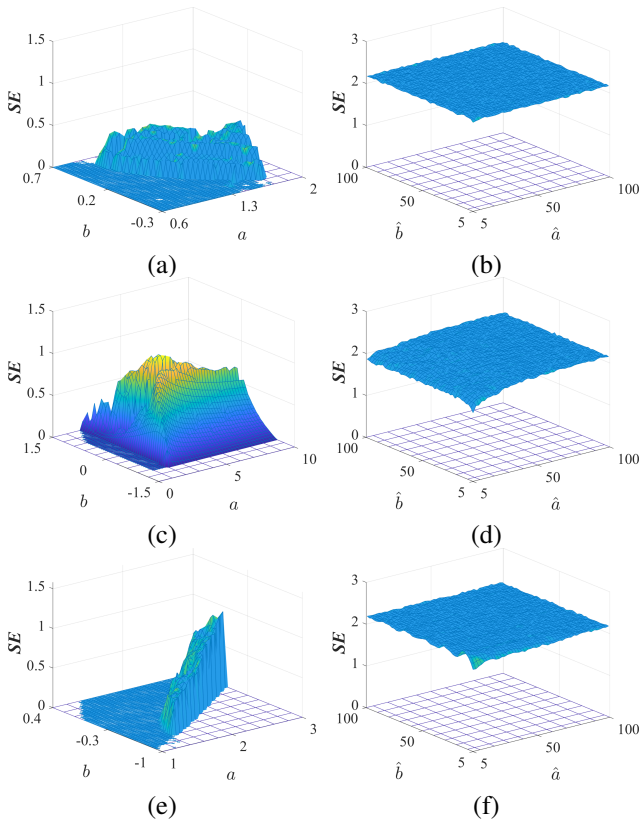$$\log_2 P(b_{i_1} b_{i_2} \cdots b_{i_K}), \tag{16}$$

Fig. 5: SEs of the time series generated by different 2D chaotic maps. (a) Hénon map; (b) improved Hénon map; (c) Zeraoulia-Sprott map; (d) improved Zeraoulia-Sprott map; (e) Duffing map; (f) improved Duffing map.

where b_{i_j} is a state of the jth signal S_j and $P(b_{i_1} b_{i_2} \cdots b_{i_K})$ is the joint probability of the K signals.

Here, we use the JE to test the uncertainty and randomness of the two signals $X = \{x_1, x_2, \cdots, x_n\}$ and $Y = \{y_1, y_2, \cdots, y_n\}$ generated by a 2D chaotic map. The JE $H(XY)$ is a positive value and its theoretical maximum can be achieved when the two signals X and Y are absolutely random and independent. This means that the joint probabilities are the multiplications of the probabilities of states, and each signal has the equal probability at each state, namely $P(b_{i_1} b_{i_2}) = P(b_{i_1}) P(b_{i_2})$, and $P(b_{i_1}) = P(b_{i_2}) = 1/M$. Thus, the theoretical maximum JE of X and Y with M states, denoted as $H(XY)_{\max}$, can be obtained as

$$
\begin{aligned}
H(XY)_{\max} &= -\sum_{i_1=1}^{M} \sum_{i_2=1}^{M} P(b_{i_1} b_{i_2}) \log_2 P(b_{i_1} b_{i_2}) \\
&= -\sum_{i_1=1}^{M} \sum_{i_2=1}^{M} P(b_{i_1}) P(b_{i_2}) \log_2 \left(P(b_{i_1}) P(b_{i_2}) \right) \\
&= -M^2 (1/M)^2 (-2 \log_2 M) \\
&= 2 \log_2 M.
\end{aligned}
\tag{17}
$$

Then, the actual JE of X and Y satisfies $0 < H(XY) \le 2 \log_2 M$, and a larger JE indicates a higher uncertainty and randomness of the two signals.

Our experiments compare the JEs of the three improved and

three existing 2D chaotic maps. For each 2D chaotic map, we set the experiment as follows. 1) randomly generate a group of initial states, ensuring that the control parameters are within the chaotic range of the chaotic map; 2) for each of the signal states $M \in \{2^1, \cdots, 2^n, \cdots, 2^8\}$, iterate the chaotic map and generate chaotic signals X and Y with length $2^{3 \times (n+1)}$; 3) calculate the JEs of X and Y for various signal states; 4) repeat steps 1) to 3) 10 times to obtain the average JEs. Table IV lists the average JEs of the three improved and three existing 2D chaotic maps under various signal states. These improved chaotic maps of 2D-MCS can obtain much larger JEs than existing chaotic maps and their JEs approach to the maximum values under various signal states. This indicates that the two chaotic signals X and Y generated by the improved chaotic maps have high uncertainty and randomness.

D. Correlation Dimension

The CD is a type of fractal dimension and it can measure the space dimensionality occupied by a time series [52]. A dynamical system is considered to have chaos properties if the CD of its time series is larger than 0, and a larger CD means a higher occupied space dimensionality of the chaotic attractors.
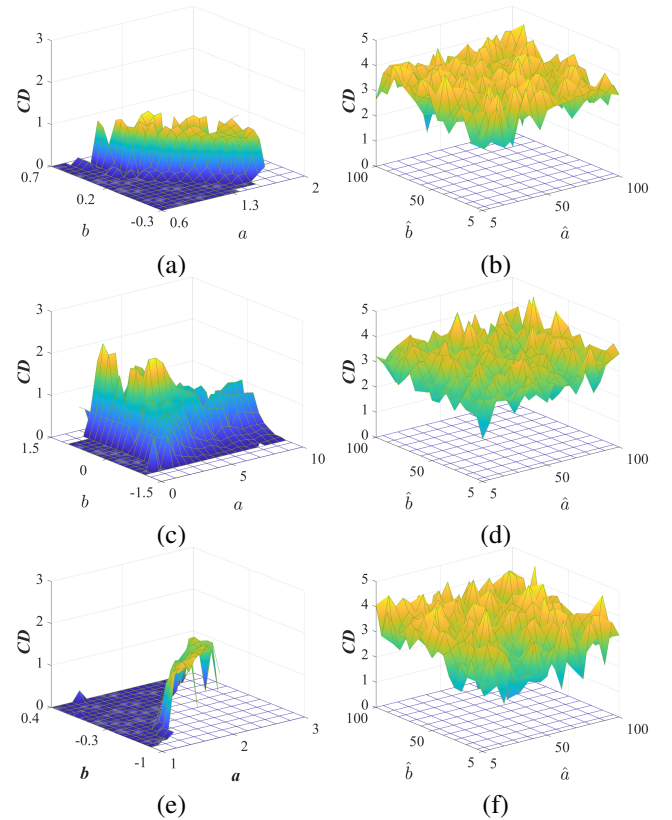

Fig. 6: CDs of the time series generated by different 2D chaotic maps. (a) Hénon map; (b) improved Hénon map; (c) Zeraoulia-Sprott map; (d) improved Zeraoulia-Sprott map; (e) Duffing map; (f) improved Duffing map.

Our experiments use the nonlinear time series analysis tool TISEAN 3.0.1[2] to calculate the CDs of the three improved

[2]https://www.pks.mpg.de/~tisean/archive_3.0.0.html

TABLE IV: Average JEs of two chaotic signals X and Y generated by different 2D chaotic maps.

	Number of signal states M							
	2^1	2^2	2^3	2^4	2^5	2^6	2^7	2^8
Hénon map	1.0487	1.9251	3.2136	4.3081	5.4064	6.5075	7.6362	8.7822
Zeraoulia-Sprott map	1.4196	2.5586	3.3279	4.1716	4.9404	5.7235	6.5439	7.2715
Duffing map	1.5125	3.3078	4.4265	5.4888	6.5010	7.4833	8.4878	9.5367
Improved Hénon map	1.9733	3.9769	5.9857	7.9920	9.9949	11.9963	13.9969	15.9971
Improved Zeraoulia-Sprott map	1.9704	3.9776	5.9844	7.9891	9.9918	11.9932	13.9939	15.9942
Improved Duffing map	1.9729	3.9831	5.9878	7.9944	9.9970	11.9985	13.9991	15.9993
$H(XY)_{max}$	2	4	6	8	10	12	14	16

and existing 2D chaotic maps. Fig. 6 shows the CDs of these chaotic maps. To make the experiment consistent, the parameter ranges of all chaotic maps are set as the same as those in LE and SE experiments. As can be observed from the experiment results, the improved Hénon, improved Zeraoulia-Sprott and improved Duffing maps can achieve positive CDs in all the parameter settings, while the existing Hénon, Zeraoulia-Sprott and Duffing maps have positive CDs only in few parameter settings. In addition, these improved chaotic maps can obtain much larger CDs than the existing chaotic maps. These results are also consistent with the LE experiment results in Fig. 4 and verify that the attractors of the improved chaotic maps of 2D-MCS can occupy a higher space dimensionality than the attractors of the existing chaotic maps.

V. Secure Communication

With the properties of unpredictability and ergodicity, chaotic systems are widely used to securely transmit data through various networks [16], [53]. When chaotic systems are used to transmit data, the distributions of their outputs greatly affect the performance of resisting transmission bit errors [54]. Because the outputs of the improved chaotic maps by 2D-MCS can fully distribute on the whole phase plane, these chaotic maps can exhibit high performance in secure communication. This section uses the RM-DCSK developed in [54] to demonstrate the performance of the improved chaotic maps by 2D-MCS in secure communication.

A. Scheme of RM-DCSK

The RM-DCSK consists of two parts: the transmitter and receiver. The transmitter first encodes the information bits using the chaotic sequence to generate transmission signal, and then sends the transmission signal to the receiver, while the receiver decodes the received signal to recover the information bits.

1) Transmitter: The structure of the transmission signal is shown as Fig. 7. As can be seen, the b_{2k} is the $2k$th information bit, $\mathbf{X}_k$ is an M-length chaotic sequence and $\mathbf{X}_k = \{x_i | 2kM < i \leq (2k+1)M\}$, where M is a spreading factor. The information bits are transmitted sequentially in equal time slots and a frame consists of two slots. For the kth frame, its first slot is the multiplication of $\mathbf{X}_k$ and b_{2k}, and its second slot is the sum of two components. The first component is the multiplication of $\mathbf{X}_k$ and the sum of b_{2k+1} and b_{2k}, and

the second component is the next chaotic sequence, namely $\mathbf{X}_{k+1}$. Thus, the kth frame of the transmission signal s_i can be represented as

$$s_i = \begin{cases} b_{2k}x_i, & 2kM < i \leq (2k+1)M \\ b_{2k+1}b_{2k}x_{i-M} + x_i, & (2k+1)M < i \leq 2(k+1)M, \end{cases}$$

where the chaotic sample x_i satisfies

$$x_{(2k+1)M+m} = x_{2(k+1)M+m}, \quad \forall k \in \{0, \pm 1, \cdots\}. \quad (18)$$
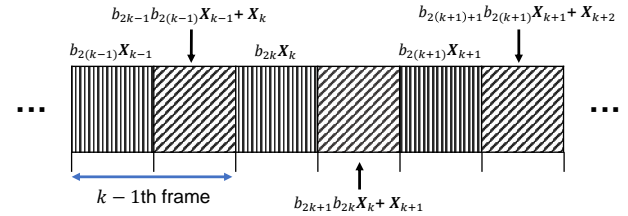

Fig. 7: Transmission signal in RM-DCSK.

Fig. 8 shows the structure of the transmitter. The component RCG is a chaotic sequence generator, and the frame combination is implemented using a delay module. As can be seen from the figure, the transmitter of RM-DCSK has a simple structure that can encode information bits to be a continuous signal s_i.
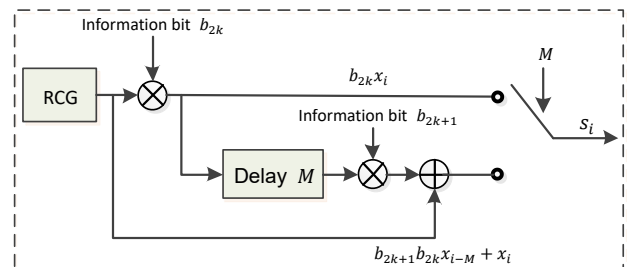

Fig. 8: Sender of RM-DCSK.

2) Receiver: When receiving the transmission signal from the transmitter, the receiver can recover the original information bits using the correlation of inner frames. Fig. 9 shows the structure of the receiver. Because signals may be contaminated by noise when transmitted in different networks, the received signal may be different from the transmission signal. Supposing that the received signal is denoted by $r_i = s_i + \xi_i$,

where ξ_i is the added noise. The correlator Z_n for recovering bit b_n is the sum of the multiplications of r_i and its delayed version r_{i-M}, namely

$$Z_n = \sum_{i=nM+1}^{(n+1)M} r_i r_{i-M}.$$

Thus, the correlator for bit b_{2k} can be calculated as

$$
\begin{aligned}
Z_{2k} &= \sum_{i=2kM+1}^{(2k+1)M} (s_{i-M} + \xi_{i-M})(s_i + \xi_i) \\
&= \sum_{i=2kM+1}^{(2k+1)M} (b_{2k-1}b_{2(k-1)}x_{i-2M} + x_{i-M} + \xi_{i-M}) \\
&\quad \times (b_{2k}x_i + \xi_i).
\end{aligned}
\tag{19}
$$

From Eq. (18), one can obtain that $x_{i-M} = x_i$. Then, the above equation can be rewritten as

$$
\begin{aligned}
Z_{2k} &= \sum_{i=2kM+1}^{(2k+1)M} (b_{2k-1}b_{2(k-1)}x_{i-2M} + x_i + \xi_{i-M})(b_{2k}x_i + \xi_i) \\
&= b_{2k} \sum_{i=2kM+1}^{(2k+1)M} x_i^2 \\
&\quad + \sum_{i=2kM+1}^{(2k+1)M} [b_{2k}b_{2k-1}b_{2(k-1)}x_i x_{i-2M} + b_{2k}x_i\xi_{i-M} \\
&\qquad + b_{2k-1}b_{2(k-1)}x_{i-2M}\xi_i + x_i\xi_i + \xi_i\xi_{i-M}].
\end{aligned}
\tag{20}
$$

The former item in the above equation is the useful information, while the latter one is the noise component. Generally speaking, the energy of the noise is much less than the energy of the useful information. Thus, the sign of Z_{2k} is determined by the sign of the information bit b_{2k}. The correlator Z_{2k+1} for information bit b_{2k+1} can be obtained similarly. Then, despite the disturbance caused by the noise, the information bit can be recovered by

$$
\hat{b}_n = \begin{cases} 1, & \text{for} \quad Z_n > 0 \\ -1, & \text{for} \quad Z_n \le 0. \end{cases}
\tag{21}
$$

B. Simulation Results

The used chaotic system in RM-DCSK greatly affects the system's performance of resisting channel noise. To demonstrate the ability of the improved chaotic maps by 2D-MCS in RM-DCSK, the chaotic sequence generator is selected as the Hénon, Zeraoulia-Sprott, Duffing, improved Hénon, improved Zeraoulia-Sprott, improved Duffing, 2D-LSC [55] and LT [56] maps, respectively. Since additive white Gaussian noise (AWGN) and additive random noise (ARN) are two types of common channel noise, we simulate RM-DCSK in the AWGN and ARN channels under different spread factors M and different levels of noise. The transmission data in each experiment are a randomly generated binary sequence with 100000-bit length. The bit error rate (BER) between the received and original data is calculated to demonstrate the ability of resisting noise.

Two groups of experiments are designed to test the BERs of RM-DCSK using different chaotic maps as the chaotic sequence generator. The first group investigates the BERs against the spread factor M. For each chaotic map, the experiments are set as follows.

1) Generate an initial state. The initial value is set as $(x_0, y_0) = (0.1, 0.1)$ for a 2D chaotic map, and $x_0 = 0.1$ for a 1D chaotic map. The system parameters are selected from the chaotic range of the chaotic map. Specifically, for a chaotic map with chaotic range (R_1, R_2) and interval L, its parameter for the i-th experiment is set as $R_1 + iL$. Table V lists the used chaotic ranges and intervals of all chaotic maps in our experiments.
2) Set the noise strength in AWGN and ARN channels as 20 dB. Simulate RM-DCSK in both noisy channels under spread factor $M \in \{10, 20, \cdots, 100\}$ and calculate the BERs.
3) Repeat the steps 1) and 2) 10 times using different initial states.
4) Calculate the average BERs of the 10 experiments.

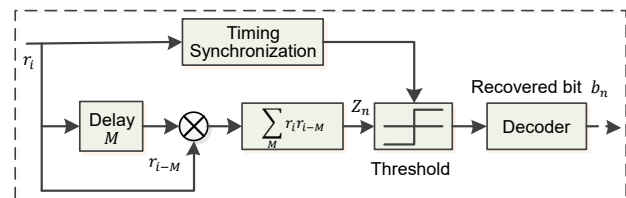Fig. 10 shows the average BERs of RM-DCSK using different chaotic maps under different spread factors M.

Fig. 9: Receiver of RM-DCSK.

TABLE V: Chaotic ranges and intervals for different chaotic maps in our experiments.

Chaotic maps	Chaotic ranges	Intervals
Hénon map	$a \in (1.16, 1.3]$	$L_a = 0.014$
	$b \in (0.2, 0.4]$	$L_a = 0.02$
Zeraoulia-Sprott map	$a \in (9, 10]$	$L_a = 0.1$
	$b \in (0.6, 0.9]$	$L_a = 0.03$
Duffing map	$a \in (2.3, 2.4]$	$L_a = 0.01$
	$b \in (-0.3, -023]$	$L_a = 0.007$
2D-LSC map [55]	$a \in (0, 1]$	$L_a = 0.1$
LT map [56]	$\mu \in (0.5, 1]$	$L_\mu = 0.05$
Improved Hénon map	$\hat{a} \in (5, 105]$	$I_{\hat{a}} = 10$
	$\hat{b} \in (5, 105]$	$L_{\hat{b}} = 10$
Improved Zeraoulia-Sprott map	$\hat{a} \in (5, 105]$	$L_{\hat{a}} = 10$
	$\hat{b} \in (5, 105]$	$L_{\hat{b}} = 10$
Improved Duffing map	$\hat{a} \in (5, 105]$	$L_{\hat{a}} = 10$
	$\hat{b} \in (5, 105]$	$L_{\hat{b}} = 10$

The second group of experiments investigates the BERs of RM-DCSK against different levels of noise. The experiments for each chaotic map are set as follows.

1) Generate an initial state using the same way as the first group of experiments.
2) Set the spread factor $M = 40$ and simulate RM-DCSK under different levels of AWGN and ARN, namely
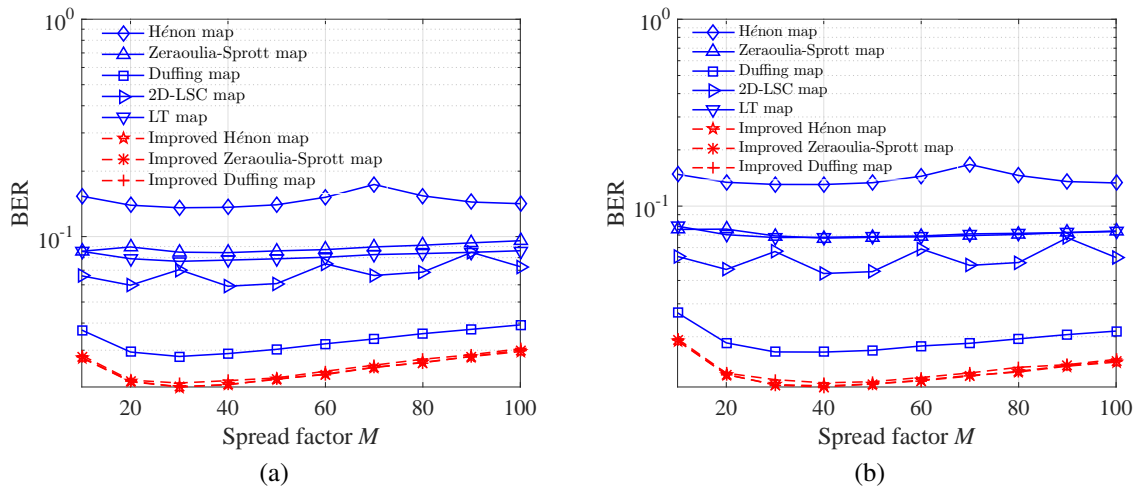
Fig. 10: BERs of RM-DCSK using different chaotic maps in the (a) AWGN channel and (b) ARN channel under the spread factor $M \in \{10, 20, \cdots, 100\}$.
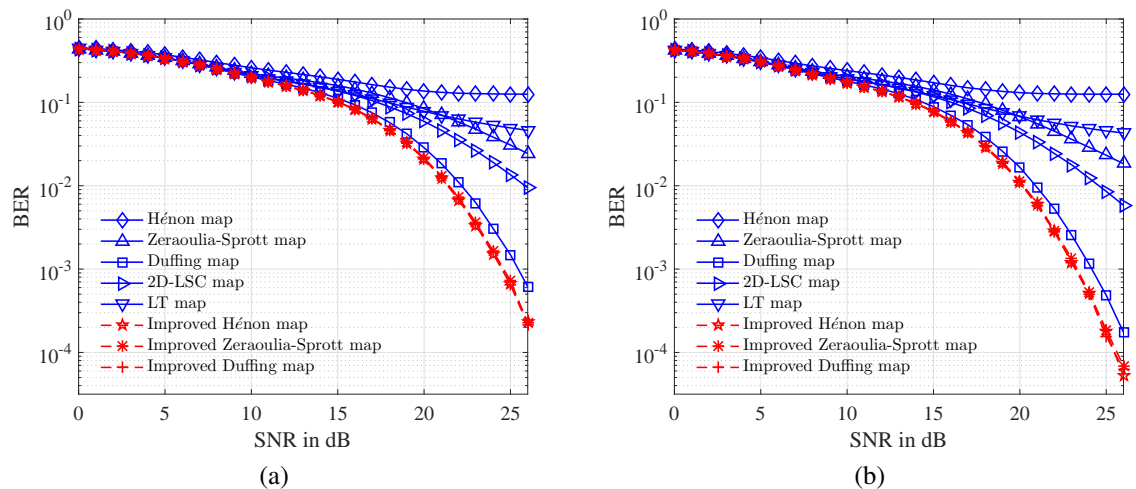

Fig. 11: BERs of RM-DCSK using different chaotic maps in the (a) AWGN channel and (b) ARN channel under the signal noise rate $SNR \in \{0, 1, \cdots, 26\}$.

$SRN \in \{0, 1, \cdots, 26\}$. Calculate the BERs of RM-DCSK under these levels of noise strength.

3) Repeat the steps 1) and 2) 10 times using different initial states.
4) Calculate the average BERs of the 10 experiments.

Fig. 11 shows the average BERs of RM-DCSK using different chaotic maps under different levels of AWGN and ARN.

One can observe from Fig. 10, under different spread factors M, RM-DCSK can always achieve much smaller BERs when using the three improved chaotic maps by 2D-MCS than using the Hénon, Zeraoulia-Sprott, Duffing, 2D-LSC [55] and LT [56] maps. Fig. 11 shows that when the signal noise ratio (SNR) is small, RM-DCSK using different chaotic maps can obtain almost the same BERs. With the increase of SNR, RM-DCSK can obtain smaller BERs when using the three improved chaotic maps than using other chaotic maps. This is because the transmission data have stronger ability of resisting channel noise when the used chaotic sequences distribute more uniformly, and the three improved chaotic maps can generate more uniformly distributed chaotic signals than other chaotic maps. Thus, the improved chaotic maps by 2D-MCS show better performance in secure communication than the original

chaotic maps and several recently developed chaotic maps.

VI. CONCLUSION

This paper scrutinized the weaknesses of the existing 2D chaotic maps. To eliminate the defects, a 2D modular chaotification system (2D-MCS) was proposed to improve the chaos complexity of existing 2D chaotic maps. The 2D-MCS adopts a modular operation as a simple transformation and applies it to the system outputs in each iteration. Three examples of improved chaotic maps were studied to demonstrate the effectiveness of 2D-MCS. The chaotic behaviors of one example of 2D-MCS are analyzed using the definition of LE. The performance evaluations show that the improved chaotic maps have much wider chaotic ranges and more complex chaotic behaviors than the original ones. To show the application of 2D-MCS, we applied the improved chaotic maps to a secure communication scheme. The experiment results demonstrate that the improved chaotic maps of 2D-MCS show better performance in resisting channel noise than the original chaotic maps and several recently developed chaotic maps. Our future work will investigate the modular chaotification to high-dimensional chaotic systems.

ACKNOWLEDGEMENT

REFERENCES

[1] S. Vaidyanathan and C. Volos, *Advances and Applications in Chaotic Systems*. Berlin, Heidelberg, Germany: Springer, 2016.

[2] X. Bu, H. Dong, Z. Wang, and H. Liu, "Non-fragile distributed fault estimation for a class of nonlinear time-varying systems over sensor networks: The finite-horizon case," *IEEE Trans. Signal Process.*, vol. 5, no. 1, pp. 61–69, Mar. 2019.

[3] P. M. S. Burt and J. H. de Morais Goulart, "Efficient computation of bilinear approximations and volterra models of nonlinear systems," *IEEE Trans. Signal Process.*, vol. 66, no. 3, pp. 804–816, Feb. 2018.

[4] S. Tong, K. Sun, and S. Sui, "Observer-based adaptive fuzzy decentralized optimal control design for strict-feedback nonlinear large-scale systems," *IEEE Trans. Fuzzy Syst.*, vol. 26, no. 2, pp. 569–584, Feb. 2018.

[5] A. Gurevich, K. Cohen, and Q. Zhao, "Sequential anomaly detection under a nonlinear system cost," *IEEE Trans. Signal Process.*, vol. 67, no. 14, pp. 3689–3703, Jul. 2019.

[6] M. W. Hirsch, S. Smale, and R. L. Devaney, *Differential Equations, Dynamical Systems, and an Introduction to Chaos*. Academic press, 2012.

[7] H. G. Schuster and W. Just, *Deterministic Chaos: An Introduction*. John Wiley & Sons, 2006.

[8] Z.-P. Wang and H.-N. Wu, "On fuzzy sampled-data control of chaotic systems via a time-dependent Lyapunov functional approach." *IEEE Trans. Cybernetics*, vol. 45, no. 4, pp. 819–829, Apr. 2015.

[9] Z. Hua, Y. Zhou, and B. Bao, "Two-dimensional sine chaotification system with hardware implementation," *IEEE Trans. Ind. Inf.*, vol. 16, no. 2, pp. 887–897, Feb. 2020.

[10] Q. Wang, S. Yu, C. Li, J. Lü, X. Fang, C. Guyeux, and J. M. Bahi, "Theoretical design and fpga-based implementation of higher-dimensional digital chaotic systems," *IEEE Trans. Circuits Syst. I*, vol. 63, no. 3, pp. 401–412, Mar. 2016.

[11] H. Esmaeili-Najafabadi, M. Ataei, and M. F. Sabahi, "Designing sequence with minimum PSL using Chebyshev distance and its application for chaotic MIMO radar waveform design," *IEEE Trans. Signal Process.*, vol. 65, no. 3, pp. 690–704, Feb. 2017.

[12] S. Chen, S. Yu, J. Lü, G. Chen, and J. He, "Design and FPGA-based realization of a chaotic secure video communication system," *IEEE Trans. Circuits Syst. Video Technol.*, vol. 28, no. 9, pp. 2359–2371, Sep. 2018.

[13] G. Li and B. Zhang, "A novel weak signal detection method via chaotic synchronization using Chua's circuit," *IEEE Trans. Ind. Electron.*, vol. 64, no. 3, pp. 2255–2265, Mar. 2017.

[14] T. Song, K. Lee, and H. Ko, "Visual voice activity detection via chaos based lip motion measure robust under illumination changes," *IEEE Trans. Consum. Electron.*, vol. 60, no. 2, pp. 251–257, May 2014.

[15] R. Bassily and S. Ulukus, "Deaf cooperation and relay selection strategies for secure communication in multiple relay networks," *IEEE Trans. Signal Process.*, vol. 61, no. 6, pp. 1544–1554, Mar. 2013.

[16] Z. Lin, S. Yu, J. Lü, S. Cai, and G. Chen, "Design and ARM-embedded implementation of a chaotic map-based real-time secure video communication system," *IEEE Trans. Circuits Syst. Video Technol.*, vol. 25, no. 7, pp. 1203–1216, Jul. 2015.

[17] S. Gong, C. Xing, S. Chen, and Z. Fei, "Secure communications for dual-polarized MIMO systems," *IEEE Trans. Signal Process.*, vol. 65, no. 16, pp. 4177–4192, Aug. 2017.

[18] Z. Xiao, S. Shan, and L. Cheng, "Identification of cascade dynamic nonlinear systems: A bargaining-game-theory-based approach," *IEEE Trans. Signal Process.*, vol. 66, no. 17, pp. 4657–4669, Sep. 2018.

[19] M. Liu, S. Zhang, Z. Fan, and M. Qiu, "H_∞ state estimation for discrete-time chaotic systems based on a unified model," *IEEE Trans. Syst., Man, Cybern. B*, vol. 42, no. 4, pp. 1053–1063, Aug. 2012.

[20] X. Zhang and J. Xu, "An extended synchronization method to identify slowly time-varying parameters in nonlinear systems," *IEEE Trans. Signal Process.*, vol. 66, no. 2, pp. 438–448, Jan. 2018.

[21] M. Xu, G. Chen, and Y.-T. Tian, "Identifying chaotic systems using wiener and hammerstein cascade models," *Mathematical and Computer Modelling*, vol. 33, no. 4-5, pp. 483–493, 2001.

[22] J.-P. Yeh, "Identifying chaotic systems using a fuzzy model coupled with a linear plant," *Chaos, Solitons & Fractals*, vol. 32, no. 3, pp. 1178–1187, 2007.

[23] J. A. Lazzús, M. Rivera, and C. H. López-Caraballo, "Parameter estimation of lorenz chaotic system using a hybrid swarm intelligence algorithm," *Physics Letters A*, vol. 380, no. 11, pp. 1164–1171, 2016.

[24] L. Lin, M. Shen, H. C. So, and C. Chang, "Convergence analysis for initial condition estimation in coupled map lattice systems," *IEEE Trans. Signal Process.*, vol. 60, no. 8, pp. 4426–4432, Aug. 2012.

[25] M. Liu, S. Zhang, Z. Fan, S. Zheng, and W. Sheng, "Exponential H_∞ synchronization and state estimation for chaotic systems via a unified model," *IEEE Trans. Neural Netw. Learn. Syst.*, vol. 24, no. 7, pp. 1114–1126, Jul. 2013.

[26] M. Xu, M. Han, T. Qiu, and H. Lin, "Hybrid regularized echo state network for multivariate chaotic time series prediction," *IEEE Trans. Cybern.*, vol. 49, no. 6, pp. 2305–2315, Jun. 2019.

[27] D. Li, M. Han, and J. Wang, "Chaotic time series prediction based on a novel robust echo state network," *IEEE Trans. Neural Netw. Learn. Syst.*, vol. 23, no. 5, pp. 787–799, May 2012.

[28] C. Li, D. Lin, J. Lü, and F. Hao, "Cryptanalyzing an image encryption algorithm based on autoblocking and electrocardiography," *IEEE MultiMedia*, vol. 25, no. 4, pp. 46–56, Mar. 2018.

[29] S. Ergün, "On the security of chaos based true random number generators," *IEICE Transactions on Fundamentals of Electronics, Communications and Computer Sciences*, vol. 99, no. 1, pp. 363–369, 2016.

[30] C. Li, B. Feng, S. Li, J. Kurths, and G. Chen, "Dynamic analysis of digital chaotic maps via state-mapping networks," *IEEE Trans. Circuits Syst. I*, vol. 66, no. 6, pp. 2322 – 2335, Jun. 2019.

[31] Y. Deng, H. Hu, W. Xiong, N. N. Xiong, and L. Liu, "Analysis and design of digital chaotic systems with desirable performance via feedback control," *IEEE Trans. Syst., Man, Cybern., Syst.*, vol. 45, no. 8, pp. 1187–1200, Aug. 2015.

[32] Z. Hua and Y. Zhou, "Exponential chaotic model for generating robust chaos," *IEEE Trans. Syst., Man, Cybern., Syst.*, doi:10.1109/TSMC.2019.2932616, 2020.

[33] L. Liu, J. Lin, S. Miao, and B. Liu, "A double perturbation method for reducing dynamical degradation of the digital baker map," *International Journal of Bifurcation and Chaos*, vol. 27, no. 7, p. artcle no. 1750103, 2017.

[34] C.-Y. Li, Y.-H. Chen, T.-Y. Chang, L.-Y. Deng, and K. To, "Period extension and randomness enhancement using high-throughput reseeding-mixing PRNG," *IEEE Trans. VLSI Syst.*, vol. 20, no. 2, pp. 385–389, Feb. 2012.

[35] H. Hu, Y. Xu, and Z. Zhu, "A method of improving the properties of digital chaotic system," *Chaos, Solitons & Fractals*, vol. 38, no. 2, pp. 439–446, 2008.

[36] S.-L. Chen, T. Hwang, and W.-W. Lin, "Randomness enhancement using digitalized modified logistic map," *IEEE Trans. Circuits Syst. II*, vol. 57, no. 12, pp. 996–1000, Dec. 2010.

[37] C. Pak and L. Huang, "A new color image encryption using combination of the 1D chaotic map," *Signal Processing*, vol. 138, pp. 129–137, 2017.

[38] Z. Hua and Y. Zhou, "One-dimensional nonlinear model for producing chaos," *IEEE Trans. Circuits Syst. I*, vol. 65, no. 1, pp. 235–246, Jan. 2018.

[39] Y. Zhou, L. Bao, and C. P. Chen, "A new 1D chaotic system for image encryption," *Signal processing*, vol. 97, pp. 172–182, 2014.

[40] Z. Elhadj and J. Sprott, "On the dynamics of a new simple 2-D rational discrete mapping," *International Journal of Bifurcation and Chaos*, vol. 21, no. 1, p. 02832, 2011.

[41] A. Mahdi, A. K. Jawad, and S. S. Hreshee, "Digital chaotic scrambling of voice based on duffing map," *International Journal of Information and Communication Sciences Communications*, vol. 1, no. 2, pp. 16–21, 2016.

[42] R. Zhang and S. Yang, "Robust chaos synchronization of fractional-order chaotic systems with unknown parameters and uncertain perturbations," *Nonlinear Dynamics*, vol. 69, no. 3, pp. 983–992, 2012.

[43] G. Chen and D. Lai, "Making a dynamical system chaotic: Feedback control of Lyapunov exponents for discrete-time dynamical systems," *IEEE Trans. Circuits Syst. I, Fundam. Theory Appl.*, vol. 44, no. 3, pp. 250–253, 1997.

[44] Wikipedia, "Chaos theory," https://en.wikipedia.org/wiki/Chaos_theory, [Online; accessed 7-September-2019].

[45] K. T. Alligood, J. A. Yorke, and T. D. Sauer, *Chaos: An Introduction to Dynamical Systems*. Springer, 2000.

[46] M. Proctor and A. D. Gilbert, *Lectures on Solar and Planetary Dynamos*. Cambridge University Press, 1994, vol. 2.

[47] O. Regev, *Chaos and complexity in astrophysics*. Cambridge University Press, 2006.

[48] L. Hogben, *Handbook of linear algebra*. Chapman and Hall/CRC, 2013.

[49] L. Dieci, R. D. Russell, and E. S. Van Vleck, "On the compuation of Lyapunov exponents for continuous dynamical systems," *SIAM journal on numerical analysis*, vol. 34, no. 1, pp. 402–423, 1997.

[50] S. Chen, S. Yu, J. Lü, G. Chen, and J. He, "Design and FPGA-Based realization of a chaotic secure video communication system," *IEEE Trans. Circuits Syst. Video Technol.*, vol. 28, no. 9, pp. 2359 –2371, 2018.

[51] J. S. Richman and J. R. Moorman, "Physiological time-series analysis using approximate entropy and sample entropy," *American Journal of Physiology-Heart and Circulatory Physiology*, vol. 278, no. 6, pp. H2039–H2049, 2000.

[52] L. Lacasa and J. Gómez-Gardeñes, "Correlation dimension of complex networks," *Physical Review Letters*, vol. 110, 2013, art. ID 168703.

[53] H.-G. Chou, C.-F. Chuang, W.-J. Wang, and J.-C. Lin, "A fuzzy-model-based chaotic synchronization and its implementation on a secure communication system," *IEEE Trans. Inf. Forensics Security*, vol. 8, no. 12, pp. 2177–2185, Dec. 2013.

[54] H. Yang and G.-P. Jiang, "Reference-modulated DCSK: a novel chaotic communication scheme," *IEEE Trans. Circuits Syst. II*, vol. 60, no. 4, pp. 232–236, Apr. 2013.

[55] Z. Hua, F. Jin, B. Xu, and H. Huang, "2D Logistic-Sine-coupling map for image encryption," *Signal Processing*, vol. 149, pp. 148–161, 2018.

[56] Y. Zhou, Z. Hua, C. M. Pun, and C. L. P. Chen, "Cascade chaotic system with applications," *IEEE Trans. Cybern.*, vol. 45, no. 9, pp. 2001–2012, Sep. 2015.

Yicong Zhou (M'07-SM'14) received his B.S. degree from Hunan University, Changsha, China, and his M.S. and Ph.D. degrees from Tufts University, Massachusetts, USA, all in electrical engineering.

He is an Associate Professor and Director of the Vision and Image Processing Laboratory in the Department of Computer and Information Science at University of Macau. His research interests include chaotic systems, multimedia security, computer vision, and machine learning.

Dr. Zhou serves as an Associate Editor for *IEEE Transactions on Neural Networks and Learning Systems*, *IEEE Transactions on Circuits and Systems for Video Technology*, *IEEE Transactions on Geoscience and Remote Sensing*, and several other journals. He is a Co-Chair of Technical Committee on Cognitive Computing in the IEEE Systems, Man, and Cybernetics Society. Dr. Zhou is a senior member of the International Society for Optical Engineering (SPIE). He was a recipient of the Third Price of Macau Natural Science Award in 2014.

Zhongyun Hua (S'14-M'16) received the B.S. degree from Chongqing University, Chongqing, China, in 2011, and the M.S. and Ph.D. degrees from University of Macau, Macau, China, in 2013 and 2016, respectively, all in software engineering.

He is currently an Associate Professor with the School of Computer Science and Technology, Harbin Institute of Technology, Shenzhen, Shenzhen, China. His research interests include chaotic system, chaos-based applications, and multimedia security.

Yinxing Zhang received the M.S. degree in Fundamental Mathematics from Guilin University of Electronic Technology, Guilin, China, in 2019.

Currently, he is a Ph.D. student with School of Computer Science and Technology, Harbin Institute of Technology Shenzhen Graduate School, Shenzhen, China. His current research interests include chaotic system and nonlinear system control.